Optical excitation function of H(1s-2p) produced by electron impact from threshold to 1.8 keV

G. K. James
Jet Propulsion Laboratory, California Institute of Technology, Pasadena, California 91109

J. A. Slevin
Department of Experimental Physics, St. Patrick's College, Maynooth, County Kildare, Ireland

D. E. Shemansky
Department of Aerospace Engineering, University of Southern California, Los Angeles, California 90089

J. W. McConkey
Department of Physics, University of Windsor, Windsor, Ontario, Canada N9B 3P4

I. Bray
Electronic Structure of Materials Centre, The Flinders University of South Australia, G.P.O. Box 2100, Adelaide 5001, Australia

D. Dziczek
Institute of Physics, Nicholas Copernicus University, 87-100 Torun, Poland

I. Kanik and J. M. Ajello
Jet Propulsion Laboratory, California Institute of Technology, Pasadena, California 91109
(Received 7 August 1996)

The optical excitation function of prompt Lyman-α radiation, produced by electron impact on atomic hydrogen, has been measured over the extended energy range from threshold to 1.8 keV. Measurements were obtained in a crossed-beams experiment using both magnetically confined and electrostatically focused electrons in collision with atomic hydrogen produced by an intense discharge source. A vacuum-ultraviolet monochromator system was used to measure the emitted Lyman-α radiation. The absolute H(1s-2p) electron impact excitation cross section was obtained from the experimental optical excitation function by normalizing to the accepted optical oscillator strength, with corrections for polarization and cascade. Our data are significantly different from the earlier experimental results of R. L. Long *et al.*, J. Res. Natl. Bur. Stand. Sect. A **72A**, 521 (1968) and J. F. Williams, J. Phys. B **9**, 1519 (1976); **14**, 1197 (1981), which are limited to energies below 200 eV. Statistical and known systematic uncertainties in our data range from $\pm 4\%$ near threshold to $\pm 2\%$ at 1.8 keV. Multistate coupling affecting the shape of the excitation function up to 1 keV impact energy is apparent in both the present experimental data and present theoretical results obtained with convergent close-coupling (CCC) theory. This shape function effect leads to an uncertainty in absolute cross sections at the 10% level in the analysis of the experimental data. The derived optimized absolute cross sections are within 7% of the CCC calculations over the 14 eV–1.8 keV range. The present CCC calculations converge on the Bethe-Fano profile for H(1s-2p) excitation at high energy. For this reason agreement with the CCC values to within 3% is achieved in a nonoptimal normalization of the experimental data to the Bethe-Fano profile. The fundamental H(1s-2p) electron impact cross section is thereby determined to an unprecedented accuracy over the 14 eV – 1.8 keV energy range. [S1050-2947(97)02202-6]

PACS number(s): 34.80.Dp, 39.10.+j, 33.20.Ni, 31.15.Ar

I. INTRODUCTION

Atomic hydrogen has been of continuous experimental and theoretical interest for well over half a century. Experimental measurements of the line spectrum have provided tests for quantum electrodynamics. Hydrogen has played a central role in atomic collision physics, primarily because hydrogen wave functions are exact and therefore a precise description of the hydrogen target is available for modeling the collision process. Atomic hydrogen, being the most abundant species, is also of great cosmological interest.

Excitation of atomic hydrogen by electron impact has been a key testing ground for the development of the theory of electron impact excitation. However, as pointed out in recent reviews by Trajmar and Kanik [1] and King *et al.* [2], significant discrepancies still remain between available experiments, as well as between experiment and theory. To a large extent this reflects the difficulty in performing experiments with atomic hydrogen, where stable, intense, and well quantified beams of the atomic species are difficult to produce. It also reflects the difficulties experienced until recently by theorists in the so-called ''intermediate-energy'' region, away from the threshold region where close-coupling calculations are reliable, and away from high energies where zero-order approximations are valid.

A measurement of the H(1s-2p) excitation cross section

(Q_{1s2p}) was carried out almost 40 years ago by Fite and Brackmann [3] in a pioneering experiment using a tungsten furnace to dissociate molecular hydrogen and an oxygen filter to isolate the Lyman-α radiation. In 1968 Long, Cox, and Smith [4] carried out a similar study, also using a tungsten furnace and oxygen filter, and normalized their data to the Born approximation at an energy of 200 eV. These data correspond to observations of Lyman-α radiation at 90° to the electron beam and require a correction for the effect of polarization in order to obtain full integral cross sections. McGowan, Williams, and Curley [5] published measurements of the H($1s$-$2p$) cross section in the threshold region primarily to observe the resonance structure. Finally, Williams [6,7] reported absolute Q_{1s2p} cross section measurements for energies between threshold and 13 eV, and for a single energy at 54.4 eV, calibrating the radiometric system in terms of the quantum yield of a freshly evaporated aluminum film and using a phase-shift analysis of the elastic scattering to determine the target hydrogen density.

Because of an extended energy range, the data of Long *et al.* [4] have been of greatest interest and the subject of much analysis by different authors. van Wyngaarden and Walters [8] corrected the Long *et al.* [4] data at all energies using Ott, Kauppila, and Fite's [9] values of polarization and Morrison and Rudge's [10] estimates of cascade from higher lying levels up to $n=5$. van Wyngaarden and Walters [8] then normalized the data by scaling the resulting experimental value to their theoretical value at 200 eV. Heddle and Gallagher [11] considered the normalization of the Long *et al.* data [4] by correcting for cascade at higher energies using the Born coefficients of Vainshtein [12] and by developing a procedure to extrapolate the experimental data onto a Bethe-Fano [13] plot. They produced corrected values and suggested that these data represent an upper limit to the true cross section, because of the remaining uncertainty in convergence to the Born high-energy dependence. Madison [14] also discussed theoretical evidence suggesting that the Long *et al.* [4] data should be reduced by approximately 5% because of the inadequacy of the Born approximation at 200 eV where their data were initially normalized. All of these analyses have led to various ''corrected'' forms of the data of Long *et al.* [4]. Thus, at the theoretically interesting energy of 54.4 eV, the Long *et al.* [4] value for Q_{1s2p} (interpolated from their data at 48.6 eV and 68.6 eV) is quoted as 0.708 a.u. (van Wyngaarden and Walters [8]) and 0.789 a.u. (Heddle and Gallagher [11]). Error bars in the original Ref. [4] values for Q_{1s2p} near 54.4 eV are stated as $\pm 1.4\%$.

Comparison of the absolute measurements of Williams [6,7] and the cross sections of Long *et al.* [4] shows that at 54.4 eV the cross section datum of Williams ($Q_{1s2p}=0.888\pm0.076$ a.u.) lies significantly higher (from 13% to 25%) than any of the corrected Long *et al.* [4] values. While in the context of experimental collision physics this may not seem a large divergence, given the combined error bars on the two measurements, this discrepancy is nevertheless viewed as significant, in part because the measurement of excitation functions of atomic hydrogen has fundamental importance for the development of theoretical models, and also in part because of the importance of the ($1s$-$2p$) Lyman-α cross sections for H and H_2 in providing secondary standards for absolute radiometric calibration (van der Burgt *et al.* [15], Shemansky *et al.* [16]).

The discrepancy between the data of Long *et al.* [4] and Williams [6,7] has provoked a sustained debate in the literature. The extensive calculations over the last few decades for excitation of atomic hydrogen have been compiled in the recent comprehensive review of Trajmar and Kanik [1] and will not be repeated here. There are two fundamental approaches to the electron scattering problem: a perturbative approach which is generally accurate at high energies and extends down to the intermediate region [the various distorted-wave Born approximations (DWBA2) of Madison and co-workers (Madison [14], Bubelev *et al.* [17]) are good examples of this approach]; a nonperturbative approach, based on an expansion of the scattering wave function in terms of a suitable set of basis states [the R-matrix approach of Burke and co-workers (Burke *et al.* [18]), and various close-coupling calculations are examples]. The most accurate theoretical data in the intermediate-energy range are likely to be the nonperturbative convergent close-coupling (CCC) calculations of Bray and Stelbovics [19], whose results lie significantly below the Williams datum at 54.4 eV but above the scaled [8] Long *et al.* [4] data. The accuracy of these calculations has been tested [19] by progressively increasing the Laguerre basis expansion of the total wave function, demonstrating an uncertainty of only a few percent in the integrated cross sections (see Ref. [20] for a review of the CCC method). These CCC calculations are supported in varying degrees by the multi-pseudo-state calculations of Callaway and Unnikrishnan [21], van Wyngaarden and Walters [8,22], Scott *et al.* [23], the second-order distorted-wave Born approximation calculations of Kingston and Walters [24], and Bubelev *et al.* [17], and the unitarized eikonal Born series (UEBS) calculations of Byron *et al.* [25], as shown in Fig. 1.

In order to resolve these outstanding discrepancies between the few available experiments, and between experiment and theory, we report here a comprehensive measurement of the prompt H Lyman-α optical excitation function produced by electron impact from threshold to 1.8 keV, together with CCC calculations performed over this extensive energy range. The raw experimental data correspond to observations of the Lyman-α signal at an angle of 90° to the incident electron beam direction and have to be corrected for polarization of the radiation, as well as cascade from higher states.

Several aspects of our measurements are significant.

(1) The extension of the excitation function measurements up to an energy of 1.8 keV allows a significantly closer approach to the dominance of the zero-order term in the first Born approximation.

(2) The present experimental approach uses a modern, efficient source of atomic hydrogen capable of producing atom densities three orders of magnitude greater than those used in the earlier experimental work.

(3) In contrast to previous work, where an oxygen filter was used to isolate the Lyman-α line, wavelength selection is achieved using a (vacuum-ultraviolet) monochromator. This not only accurately isolates the Lyman-α emission, but also greatly increases the accuracy of the determination of the molecular contribution to the observed photon signal.

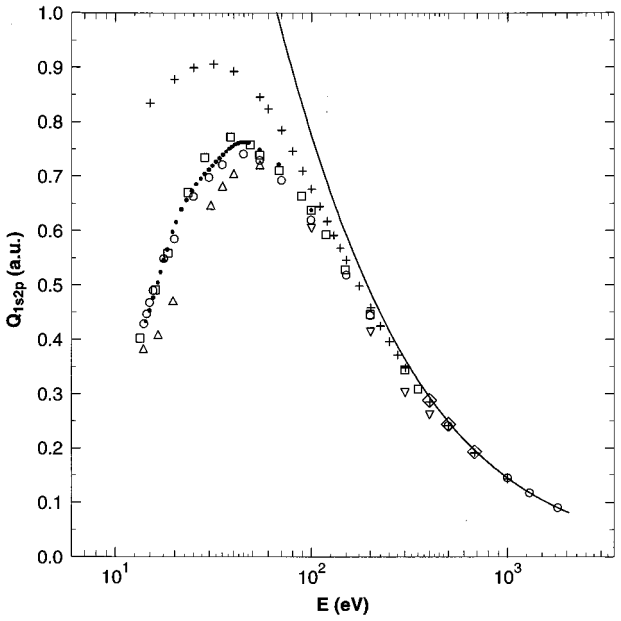

FIG. 1. Summary plot of theoretical H(1s-2p) cross sections. The calculation methods can be categorized into various approaches: Born approximation (solid curve) [Eq. (9a)]; present convergent close coupling (CCC) calculations (open circles); multi-pseudo-state calculations of van Wyngaarden and Walters [8,22] (open squares), Scott *et al.* [23] (up triangles), Callaway and Unnikrishnan [21] (dots); second-order distorted-wave Born approximation (DWBA2) calculations of Kingston and Walters [24] (open diamonds), Bubelev *et al.* [17] (pluses); unitarized eikonal Born series (UEBS) calculations of Byron *et al.* [25] (down triangles).

(4) We have used a stable, high efficiency Lyman-α detector based on a cesiated channeltron with a quantum efficiency of 15% at 121.6 nm.

II. APPROACH AND THEORETICAL BACKGROUND

The determination of integral cross sections for optically allowed transitions from observations of the radiation emitted at either 90° or at the ''magic angle'' 54.7° with respect to the incident electron beam direction has a long and well established history (Heddle and Gallagher [11], van der Burgt *et al.* [15], Filipelli *et al.* [26]). Here we provide a brief description of the method.

A beam of hydrogen atoms, effusing from a radio-frequency (rf) dissociator, is crossed by a beam of electrons of variable energy and observations are made of the Lyman-α emission at 90° using a vacuum-ultraviolet (VUV) monochromator for wavelength selection. At sufficiently low pressures, where radiationless deactivation and self-absorption effects can be neglected, a simple relationship relating the rate of total photon emission I in a transition from a state j to a final state i can be written

$$I_{ji} = i_e n_i L Q_{ji}, \tag{1}$$

where i_e is the electron beam current in electrons per second, n_i is the number density of the target gas, L is the effective path length of the electron beam through the target, and Q_{ji} is the integral cross section for the emission process. Thus an absolute measurement of the intensity I_{ji} radiated in all directions gives the integrated cross section, provided the other experimental parameters in Eq. (1) are known. In general the upper level j is populated indirectly by radiative cascade, as well as directly from state i. Thus to obtain the direct integral cross section for excitation (Q_{ij}) from the ground state, it is necessary to make corrections for cascade transitions.

The rate of photon emission at an angle θ to the electron beam is given by

$$I_{ji}(\theta) = \frac{I_{ji}}{4\pi}\left[\frac{1 - P\,\cos^2\theta}{1 - P/3}\right], \tag{2}$$

where P is the polarization of the emitted radiation and characterizes the anisotropy of the emission process. The present experimental geometry involves observations at 90°. Thus we obtain

$$I_{ji} = 4\pi I_{ji}(90°)(1 - P/3). \tag{3}$$

A measurement of $I_{ji}(90°)$ yields an apparent cross section $Q_j(90°)$ which must be corrected to obtain the true integrated cross section.

It is not possible to determine all the factors in Eq. (1) absolutely, requiring a suitable normalization procedure in order to place the relative measurements on an absolute scale. One of the most widely used techniques for this purpose is to normalize the data to the Born approximation at sufficiently high energy where its validity is assumed while ensuring that the electron and atom beam overlap does not vary significantly as the incident electron energy is ramped from higher to lower energies. Two different techniques using this basic approach are presented in the analysis of the present experiment. A conventional normalization procedure using a Bethe-Fano plot was applied in the manner described by Heddle and Gallagher [11] in which the experimental data are scaled to approach the asymptotic limit at high energy defined by the Bethe-Fano line. The slope and intercept of this Bethe-Fano line are defined for an uncoupled (1s-2p) system. A normalization procedure using a nine-parameter analytic fitting function which is sensitive to the subtle effects of any multistate coupling is also presented. The limiting factor in obtaining high accuracy in cross section measurement in this case is the influence of multistate coupling which extends to unusually high energy (~1 keV) for the H(1s-2p) excitation process.

Analytic methods

The first Born approximation for electric dipole excitation by electron impact is described by Mott and Massey [27] in the form of the momentum transfer integral,

$$Q_{ij} = \frac{4\pi a_o^2 z^2}{E}\int_{\zeta_{\min}}^{\zeta_{\max}} \frac{f_{ij}(K)\,d\zeta}{E_{ij}\zeta}, \tag{4a}$$

where

$$\zeta = (K a_o)^2, \tag{4b}$$

$$\Omega_{ij}=\omega_i E\frac{Q_{ij}}{\pi a_o^2 z^2}, \tag{4c}$$

$$\Omega_{ij}=4\omega_i\int_{\zeta_{\min}}^{\zeta_{\max}}\frac{f_{ij}(K)d\zeta}{E_{ij}\zeta}. \tag{4d}$$

In these equations Q_{ij} is the excitation cross section, a_o is the Bohr radius, z is the nuclear charge of the target, E is the energy of the impacting particle in Rydbergs, $f_{ij}(K)$ is the generalized oscillator strength for transition from state i to state j, K is the momentum transfer magnitude, and ω_i is the lower state degeneracy. A more convenient working relationship is used in Eqs. (4c) and (4d) in which the momentum transfer integral is related to the fundamental collision strength quantity Ω.

The range of ζ is given by the relations

$$\zeta_{\max}=2E\left(\frac{\mu}{m}\right)^2\left\{1-\frac{1}{2}\frac{m}{\mu}\frac{1}{X}+\left[1-\frac{m}{\mu}\frac{1}{X}\right]^{1/2}\right\}, \tag{5a}$$

$$\zeta_{\min}=2E\left(\frac{\mu}{m}\right)^2\left\{1-\frac{1}{2}\frac{m}{\mu}\frac{1}{X}-\left[1-\frac{m}{\mu}\frac{1}{X}\right]^{1/2}\right\}, \tag{5b}$$

$$X=\frac{E}{E_{ij}}. \tag{5c}$$

X is the dimensionless energy, μ is the reduced mass of the collision complex, and m is the mass of the impactor. If the impacting particle is an electron the relationships reduce to

$$\zeta_{\max}=2E_{ij}X\left[2-\frac{1}{X}-\frac{1}{8}\frac{1}{X^2}-\cdots\right], \tag{6a}$$

$$\zeta_{\min}=\frac{1}{4}\frac{E_{ij}}{X}\left[1+\frac{1}{2}\frac{1}{X}+\frac{5}{16}\frac{1}{X^2}+\cdots\right]. \tag{6b}$$

Contrary to the statement by Inokuti [28], both limits must be applied to the integral in order to obtain an accurate derivation of the Born approximation (Ref. [29]). For the H($1s$-$2p$) transition, the generalized oscillator strength is given by [27]

$$f_{12}(K)=E_{12}\times 2^{15}\times 3^{-10}\frac{1}{(1+\frac{4}{9}\zeta)^6}. \tag{7}$$

The substitution of Eq. (7) into Eq. (4d) yields

$$\Omega_{12}=C_7\int_{\zeta_{\min}}^{\zeta_{\max}}\frac{d\zeta}{\zeta(1+\frac{4}{9}\zeta)^6}, \tag{8a}$$

$$C_7=4\omega_i M_{ij}^2, \tag{8b}$$

$$M_{ij}^2=\frac{f_{ij}}{E_{ij}}, \tag{8c}$$

$$\Omega_{12}=C_7\left[\ln\left(\frac{\zeta}{1+\frac{4}{9}\zeta}\right)+\sum_{i=1}^{5}\frac{1}{i}\frac{1}{(1+\frac{4}{9}\zeta)^i}\right]_{\zeta_{\min}}^{\zeta_{\max}}, \tag{8d}$$

where M_{ij} is the dipole matrix element. The relation (8d) differs from the equivalent equation (4.6) given in Inokuti [28]. In approximation, Eq. (8d) reduces to

$$\Omega_{12}=C_5+\frac{C_6}{X}+C_7\ln(X), \tag{9a}$$

$$C_5/C_7=0.2021, \tag{9b}$$

$$C_6/C_7=0.7501, \tag{9c}$$

$$C_7=4.447. \tag{9d}$$

The normalization procedure described in detail by Heddle and Gallagher [11] essentially forces the experimental collision strength data [plotted against $\ln(E)$] to approach a Bethe-Fano line asymptotically at high energy. The formulation for this Bethe-Fano line is equivalent to relation (9a) but without the C_6 term. The slope (determined from the constant C_7) is related to the accepted optical oscillator strength and the energy intercept is fixed using the Born value of C_5 for an uncoupled system.

In an alternative normalization approach, a modified Born analytic function is used [16,30] to fit the collision strength curve over the entire range of energy. This is given by the equation

$$\Omega_{ij}=\frac{C_0}{X^2}+\sum_{k=1}^{4}C_k\exp(-kC_8X)+C_5+\frac{C_6}{X}+C_7\ln(X), \tag{10}$$

where the additional terms with constants C_0–C_4, C_8, represent electron exchange and configuration mixing contributions to the total collision strength. A resonance component at threshold [6] is not included in Eq. (10), but will be treated in a future paper [31]. The analytic fitting technique has advantages over the conventional Bethe-Fano procedure: (1) It provides a measure of the magnitude of the deviation from the Born approximation at high energies caused by the influence of multistate coupling, and (2) the best fit function utilizes the entire energy range determining the shape function of the experimental data.

Analysis of the present CCC calculations using Eq. (10) leads to a range of values of the coefficients, depending on the high-energy truncation of the data set. This variation as discussed further below is an indicator both of the heavy correlation of terms and limitation in accuracy of the CCC calculations at the few percent level. This fact sets a fundamental limit on the ability to obtain independent accurate experimental measurements of the H($1s$-$2p$) cross section through analysis of the shape function (energy dependence of collision strength) in spite of the extension of the measurements to 1.8 keV.

The generalized oscillator strength [Eq. (7)] is based on the uncoupled properties of the $1s$-$2p$ configuration. As we show below, the $1s$-$2p$ excitation function both experimentally and theoretically has the characteristics of a heavily coupled system that extends over a broad impact energy range, indicating substantial deviation from the shape of Eq. (7). The terms in Eq. (9a) that depend on the shape of the generalized oscillator strength, C_5 and C_6, therefore should

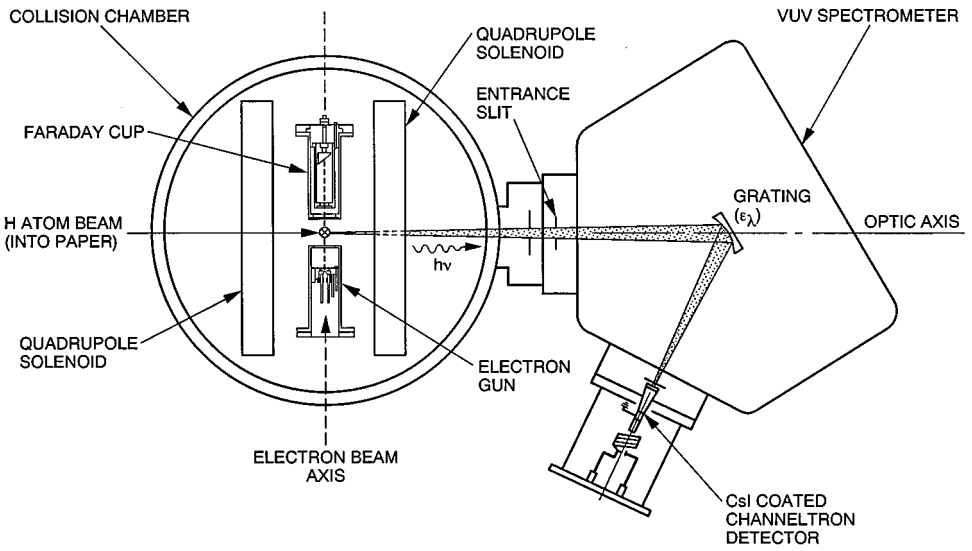

FIG. 2. Schematic top view of the experimental apparatus showing the electron impact collision chamber in tandem with a 0.2 m VUV monochromator and CsI-coated channeltron detector. A three element electron gun is shown in which the beam is confined by the axial magnetic field produced by four solenoids arranged in a quadrupole configuration. This magnetic gun is used for measurements from threshold to 200 eV. An electrostatic electron gun (Fig. 3) is used for measurements from 200 to 1800 eV. The atomic H beam is produced by the rf discharge source shown in Fig. 4. Note that for the present measurements the spectrometer is rotated by 45° about the optic axis from the indicated orientation, as shown in Fig. 5.

not be regarded as accurate quantities. There is no indication that the optical oscillator strength calculated from the Coulomb approximation (Refs. [32,33]) is measurably affected by coupling, and we assume that the value of C_7 is accurately determined by Eq. (9d).

III. EXPERIMENT

A. Apparatus

The experimental crossed-beams apparatus is shown schematically in Fig. 2. It consists of an electron impact chamber equipped with an atomic hydrogen source, in tandem with a 0.2 m vuv monochromator (resolving power 250) and CsI-coated channeltron detector positioned after the exit slit of the monochromator. Two very different electron guns have been used in the present experiment: a relatively simple three element gun which uses magnetic field confinement and a six element electrostatic gun, designed and constructed by Kimball Physics, Inc. [34]. The magnetic gun, shown in Fig. 2, was used for low-energy measurements, while the electrostatic gun (Fig. 3) was used for the higher energies. The use of two different gun designs is crucial to the success of the present experiment. To achieve the correct normalization, it

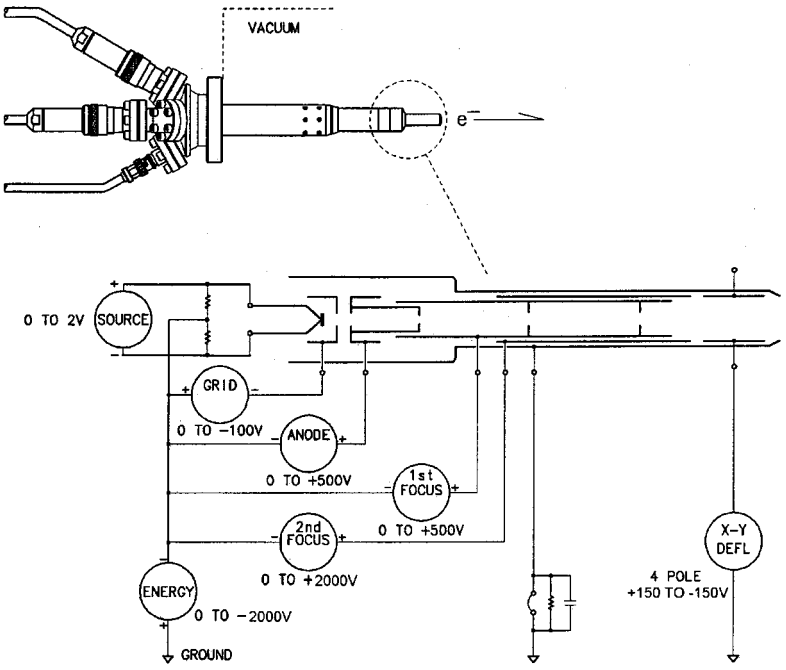

FIG. 3. Schematic diagram of the electrostatic electron gun and associated electronics [34]. A unipotential tungsten cathode produces an electron beam of low energy spread (~0.3 eV). The lens design enables a constant focal plane position and spot size to be maintained over the energy range in which measurements are made (0.2–1.8 keV). Typical beam currents are ~5 μA. The X and Y deflectors provide beam steering capability.

is essential to measure the very weak signals at high energies to high accuracy. Since the confining magnetic field traps secondary electrons from ionization processes, and further since the magnetic gun design is such that a small number of low-energy secondaries are inevitably produced from collisions at high energies with the gun apertures, it is essentially impossible to reach the Born limit at high energies with a magnetic gun. Thus a well designed electrostatic gun is essential for the high-energy measurements. On the other hand, it is difficult to maintain a constant beam cross section down to the lowest energies using an electrostatic gun, and the experimental signal is sensitive in the present experiment to any change in the electron-beam–atom-beam overlap. Variations in the size of the electron beam are minimized by the use of magnetic field confinement. It should be noted that use by Ref. [4] of an electrostatic gun at low electron impact energies was possible since the atomic H target was a beam of essentially uniform density, eliminating systematic effects due to variation in electron beam profile with energy.

The magnetic electron gun and monochromator systems have been described in detail in earlier publications [35,36]. Thermionic electrons produced by heating a tungsten filament are extracted by a Pierce electrode and extractor lens combination and accelerated or decelerated by an aperture lens (or anode) to achieve the final energy. The electron beam is collimated by the axially symmetric magnetic field (60 G) produced by a quadrupole solenoid arrangement. Ramping of the electron beam energy is controlled by a multichannel analyzer (MCA), and the data are accumulated in the MCA memory.

The electrostatic gun was custom designed as a complete subsystem by Kimball Physics, Inc. and uses a unipotential refractory metal cathode to produce a beam of low-energy spread ($\sim$0.3 eV). By use of multistaging and a computer-designed zoom lens, a constant focal plane position is maintained over the energy range from 10 eV to 2.0 keV, with a constant spot size ($\sim$1.3 mm diameter) in the range 50–1800 eV. The direction of the output beam can be controlled by a set of X and Y deflectors. Currents of $\sim$5 μA are typical at all energies. Programmable power supplies provide voltages for all of the gun elements. The entire gun operation is controlled by a personal computer (PC) operating in a Lab Windows [37] environment.

A deep Faraday cup (aspect ratio $\sim$10:1), designed to eliminate backscattered secondary electrons, is used to collect and monitor the electron beam current. The rear surface of the inner Faraday cup is electrically isolated from the outer cylinder and is coated with carbon soot. By suitable biasing (typically the inner cup is at $+60$ V and the outer cylinder at $+10$ V), more than 99% of all the current appears in the inner Faraday cup at all energies, the remainder being collected on the outer cylinder. Measurements of the Lyman-α signal were carried out for a large range of bias voltages and electron energies to ensure that any field penetration of cup voltages into the interaction region did not lead to quenching of metastable atoms within the field of view of the detection system. No effect was observed, indicating that field penetration from the Faraday cup was not a significant effect.

The atomic hydrogen source has been described in detail by Slevin and Stirling [38] and is shown in Fig. 4. Hydrogen

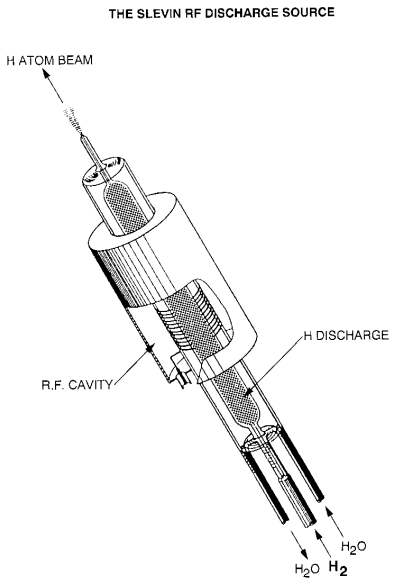

FIG. 4. Schematic diagram of the rf discharge source (Ref. [38]). Molecular hydrogen (purified by passing through a palladium finger) is dissociated in a discharge excited within a rf cavity, resonant at 36 MHz. The Pyrex discharge tube is water cooled. A typical dissociation fraction, measured at the interaction region, is 0.65 $\pm$0.02.

molecules are dissociated in a discharge, excited within a rf cavity, resonant at 36 MHz. Hydrogen atoms effuse from the water-cooled Pyrex discharge tube, past a VUV photon trap, and through a 1 mm capillary into a field-free interaction region where they are crossed with the electron beam. Photons emitted from the interaction region and orthogonal to the electron and atom beams are wavelength selected by a VUV monochromator with slit widths chosen to ensure adequate separation of atomic line emissions. This radiation is detected by a channeltron, coated with a suitable CsI layer to enhance quantum efficiency at 121.6 nm. The effectiveness of the photon trap in preventing stray photons, generated within the discharge tube, from being detected was verified by measuring the spectrum produced in the absence of the exciting electron beam. No measurable Lyman-α radiation was detected under these conditions.

The VUV monochromator system is rotated such that the plane defined by the monochromator entrance slit and optic axis is at 45° to the electron beam axis (see Fig. 5). This orientation removes polarization effects that may be induced by the monochromator and detector systems, as described by Clout and Heddle [39] and Donaldson *et al.* [40].

Precise wavelength selection, using the VUV monochromator, is a critical factor in quantifying the molecular contribution to the observed Lyman-α signal. The use of an oxygen filter in the previous work of Long *et al.* [4] and Williams [6,7] introduces uncertainty as to precisely what spectrum is transmitted to the detector. An oxygen filter has a transmission window that spans several molecular emissions. It is difficult in practice to accurately estimate the molecular content in the observed signal when an oxygen filter is used, due to the unavailability of accurate absorption data for the high pressures at which these filters are used. This uncertainty contributed to the large systematic error

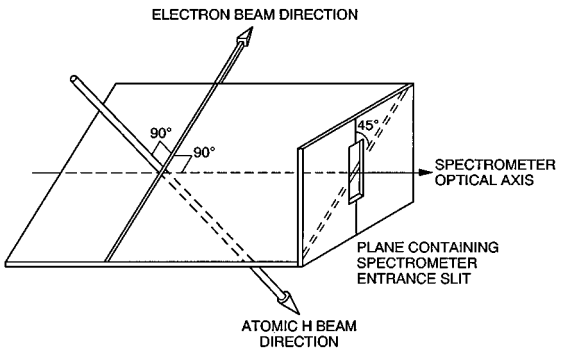

FIG. 5. Orientation of the electron and atom beams with respect to the monochromator (Ref. [40]). By rotating the monochromator such that the plane defined by the entrance slit and optic axis is at 45° to the electron beam axis, effects due to the polarization sensitivity of the detection system are eliminated.

found for the dissociative cross section for Lyman-α from H_2 used as a calibration standard for many years [16]. The use of a monochromator will enable future measurements of the excitation functions of other members of the Lyman series to be made with the present apparatus.

The entire experimental system is interfaced to a PC which monitors all important experimental parameters and controls the electron beam energy in the case of the electrostatic gun. Measured signals are normalized to the electron beam current and hydrogen source pressure (measured by a very stable and accurate Varian model CHMX-11-001 capacitance manometer), eliminating variations in these quantities as sources of systematic error. Data are accumulated in a multiple scanning mode to reduce the effects of drift in other experimental parameters.

B. Correction procedure for polarization

Lyman-α signals measured at 90° are corrected for polarization in the manner described in Sec. II in order to take account of deviations from an isotropic distribution and obtain values for the integral cross section. In the region from threshold to 200 eV, the values for polarization measured by Ott *et al.* [9] were used to correct our experimental data. At energies above 200 eV, the polarization calculations of McFarlane [41] were used. Reference [41] employed a Born procedure to find values for polarization P which are represented by the formula

$$P=\frac{P_0[3-\ln(E/E_0)]}{(2-P_0)\ln(E/E_0)+P_0}, \tag{11}$$

where $E_0=8.337$ eV and $P_0=0.42$ is the threshold polarization [42].

We use the above dichotomy, in spite of the availability of data from Ott *et al.* [9] above 200 eV, because the Ott data have relatively large errors in this region and we believe the McFarlane data are more reliable. However, it should be emphasized that whatever approach is taken to this polarization correction, the correction itself is not large, ranging from a maximum of 8% at low energies to 3% at the highest energies.

C. Correction procedure for molecular emission contamination

Since the hydrogen beam is not fully dissociated, the observed photon signal at Lyman-α, obtained with the rf discharge, contains a contribution from molecular emission which must be quantified and subtracted in order to obtain the net $(e+H)$ excitation function. The molecular component results from Lyman-α radiation produced by dissociative excitation of the molecule, as well as radiation from molecular bands transmitted by the bandpass of the monochromator [full width at half maximum (FWHM) 2.4 nm at typical slit widths of 600 μm]. In order to correct the measured excitation function for this molecular contribution, the dissociation fraction must be measured, together with the corresponding excitation function with the discharge off.

The dissociation fraction is established in the manner described by Forand *et al.* [43] by tuning the monochromator to a H_2 molecular band at 110.0 nm (with the bandpass adjusted to exclude any atomic component from Lyman-α or Lyman-β) and measuring the molecular emission with the discharge on and off at the same hydrogen source driving pressure and electron beam current. The dissociation fraction D is the ratio of atoms to the total number of particles in the beam and is related to these two signals S_1 (discharge on) and S_2 (discharge off) by the relationship

$$D=1-\left(\frac{T_2}{T_1}\right)^{1/2}\frac{S_1}{S_2}, \tag{12}$$

where T_1 and T_2 are the effective kinetic temperatures in the gas beam with the discharge on and off, respectively. Woolsey *et al.* [44] and Forand *et al.* [43] measured these kinetic temperatures in an identical source and found that the two temperatures were equal, confirming the reasonable assumption that the source indeed thermalizes the hydrogen beam.

Once the dissociation fraction has been established, the net $(e+\mathrm{H})$ Lyman-α signal S_H can be obtained from measurements of S_1 and S_2 made at Lyman-α with the discharge on and off, respectively, using the relationship derived by [43]

$$S_H=S_1-(1-D)S_2. \tag{13}$$

This correction procedure is applied at each electron impact energy by measuring excitation functions under the same conditions with the discharge on and off.

Typical VUV emission spectra produced by electron impact at 100 eV with the rf discharge on and off are shown in Fig. 6 at a spectral resolution of 0.5 nm (FWHM). The same molecular subtraction procedure used for the excitation function data can be applied to these spectra, yielding the net $(e+H)$ spectrum also shown in Fig. 6. Lyman series members up to $n=6$ can be clearly identified in our net $(e+H)$ spectrum, together with the series limit at 91.113 nm. The molecular bands around 110.0 nm used in the determination of the dissociation fraction can be seen in the spectrum of the undissociated molecular beam. A typical value for the measured dissociation fraction is 0.65 ± 0.02.

D. Resonance trapping

Since the H(2p) excited state connects radiatively with the ground state, it is critical to ensure that the excitation

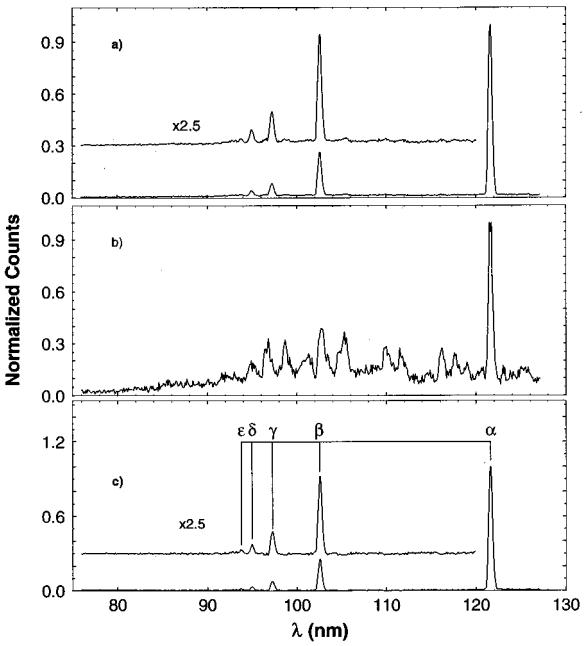

FIG. 6. Emission spectra produced by electron impact excitation at 100 eV of a partially dissociated target beam (discharge on) and an undissociated molecular target beam (discharge off) are shown in (a) and (b), respectively, at a resolution of 0.5 nm (FWHM). Application of the molecular subtraction procedure described in Sec. III yields the net $(e+H)$ spectrum shown in (c) in which Lyman series members up to $n=6$ can be identified.

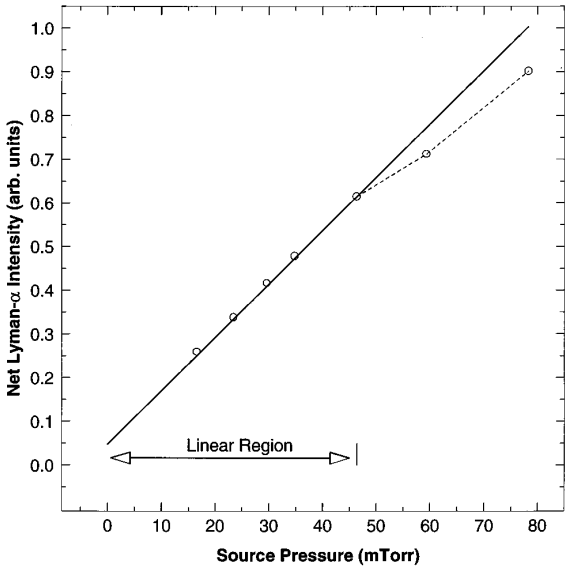

FIG. 7. Plot showing the net $(e+H)$ Lyman-α intensity measured at 100 eV as a function of discharge source pressure. The dissociation fraction is measured at each pressure together with the signals obtained with the discharge on and off. Net $(e+H)$ Lyman-α intensities are obtained using the procedure described in Sec. III. Operation of the source at pressures less than $\sim$46 mTorr ensures the absence of resonance trapping effects.

function measurements are free from resonance radiation trapping effects. Operating under Knudsen conditions at the beam source preserves a linear relationship between the source pressure and the number density in the interaction region. Figure 7 illustrates the relationship between the source pressure (measured by the Varian capacitance manometer) and the Lyman-α signal detected at 100 eV. These data verify the absence of resonance radiation trapping for source pressures less than 46 mTorr, where the detected photon signal is proportional to the hydrogen source pressure. All of the measurements reported here were obtained at hydrogen pressures of $\sim$40 mTorr.

E. Cascade correction

The observed Lyman-α photon signal includes a contribution from the decay of higher lying states cascading into the $2p$ state. This has been calculated using an atomic hydrogen model constructed to the $n=9$ level, with a collisional radiative equilibrium code [45,31], which establishes the emission line intensities for the entire system to a selected principal quantum number upper limit, providing an exact calculation of the cascade contribution to the measured cross sections. Cross sections in the model for the np orbitals have been calculated in the present work by scaling the $(1s\text{-}2p)$ cross section obtained with the CCC theory, according to the oscillator strength of the transition. Excitation cross sections to the ns and nd levels have also been derived from the same calculations. The cascade contribution has been established as an analytic function using Eq. (10) with coefficients given in Table I.

The cascade contribution calculated here has been compared to the calculated cascade corrections based on the Morrison and Rudge [10] formulation for levels up to $n=5$, using the CCC calculations, with excellent agreement.

Figure 8 shows the integrated cascade cross section feeding the H$(2p)$ state, calculated by Ref. [31], and the correction to the measured H$(1s\text{-}2p)$ collision strength. The experimental data shown in Fig. 8 have been corrected for the effect of polarization and normalized using the analytic fitting procedure described in Sec. IV. The cascade correction to the H$(1s\text{-}2p)$ cross section is significant near threshold.

TABLE I. Collision strength coefficients.

Coefficient[a]	Born[b]	Experiment[c]	Theory[d]	Theory[e]	Cascade[f]
C_0		-6.0221		-3.6969	-3.3707
C_1		-8.6381	-10.387	-7.1941	3.7832
C_2		15.988	30.798	3.8606	6.8398
C_3		-16.566	-53.092	-4.0690	21.950
C_4			38.965		
C_5	0.8988	-0.29151	0.12536	-1.0997	0.36692
C_6	3.3358	14.161	-0.73427	11.159	0.41985
C_7	4.447	4.447	4.447	4.7500	0.055239
C_8		0.060256	0.17990	0.1349	1.1220

[a]See text, Eq. (10).

[b]H$(1s\text{-}2p)$; Born approximation, Eq. (9a).

[c]H$(1s\text{-}2p)$; present work.

[d]H$(1s\text{-}2p)$; analysis of the CCC calculations to 200 eV, fixing the value of C_7 by the value of f_{ij}.

[e]H$(1s\text{-}2p)$; analysis of the CCC calculations to 2 keV.

[f]H$(1s\text{-}nl) \rightarrow$ H$(2p \leftarrow nl)$; calculated cascade into the H$(2p)$ state (Ref. [31]), see text.

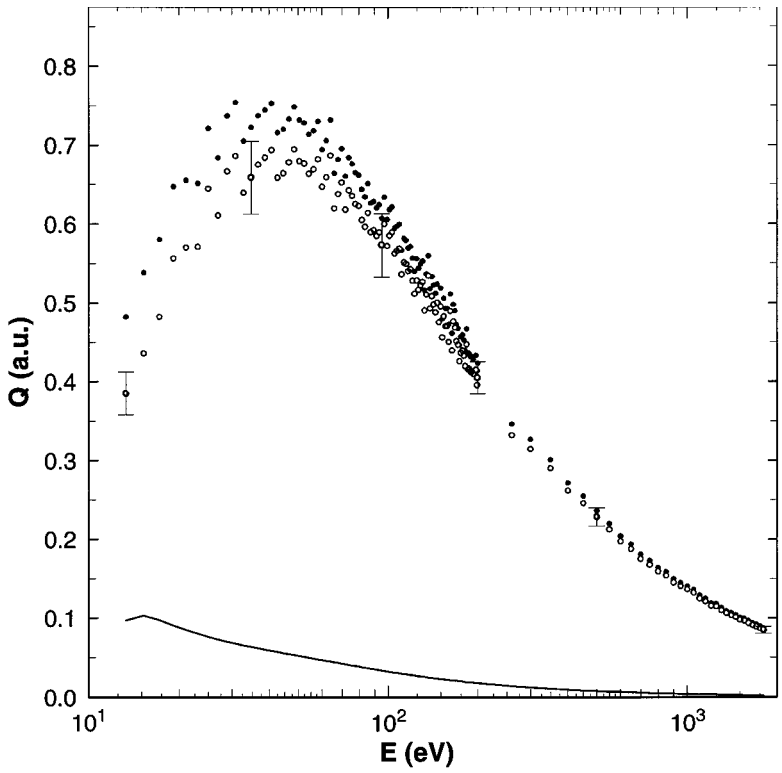

FIG. 8. The effect of cascade on the measured H($2p$) cross section. The calculated (Ref. [31]) cascade cross section for populating the H($2p$) state by electron excitation, shown as a solid line, compared to the experimental H($1s$-$2p$) emission cross section, shown as solid circles. The experimental data have been corrected for polarization effects, and normalized using the analytic fitting procedure described in Sec. IV. The open circles are the experimental data after subtraction of the calculated cascade.

At energies below 20 eV the correction is in excess of 15% and at 14 eV the contribution is 27%.

It is important to ensure that the calculated cascade fractions are applicable to our particular experimental configuration. It has been pointed out by Van Zyl and Gealy [46] that very small electric fields can greatly perturb calculated cascade fractions. The precautions, indicated earlier, taken to exclude stray fields from the interaction region to prevent quenching of H($2s$), should also ensure that perturbing effects of this type are not present in our experiment. These factors are discussed in detail in the Appendix.

A further effect which must be considered when using the magnetically collimated gun is the motional electric field experienced by the moving atoms in the magnetic field. This effect has been considered by Van Zyl *et al.* [47]. They show that motional fields as low as 1 V/cm can have significant state-mixing effects with a consequent impact on the decay channels, particularly for $n>4$. For atomic hydrogen atoms of 50 meV energy, a motional electric field of $\sim$0.3 V/cm is estimated at a field $B=100$ G. Calculations show that if fields of 1 V/cm are assumed, the cascade contribution will be reduced by at most 5%. Van Zyl *et al.* [47] also comment on the fact that Zeeman splitting of the levels in a magnetic field could affect the branching ratios for the decay. They suggested that this effect should be small for fields less than a few gauss. Since this effect would be most pronounced for the higher n levels, when the cross sections are very small, we anticipate an insignificant effect on the cascade contribution in the present experiment.

All of the above assumes that the cascade radiation is unpolarized. The main contribution to any polarization of the cascade radiation comes from the nd states where the radiation is normally very weakly polarized. The overall effect of polarization of the cascade radiation is therefore expected to be very small, less than 1% in the worst case at low energies.

We note that the dwell time of atoms in the field of view of the spectrometer is about 2 μsec. This eliminates excited atoms in states above $n=8$ as contributors to cascade into the H($2p$) state.

IV. ANALYSIS OF DATA

A. Experimental data

As described in Sec. III, the experimental data were obtained in two groups using different electron gun designs. The lower-energy region was explored using the magnetically collimated gun to an upper limit in energy of 200 eV. Beyond 200 eV to the peak beam energy of 1.8 keV the relative cross sections were obtained using the electrostatic electron gun. The combined statistical and known systematic uncertainties in the measurements have been estimated to range from 4% at energies near threshold to 2% at 1.8 keV. Details of the error analysis are provided in the Appendix. The electron beam energies were established in absolute value at low energy by using the sharp threshold for the dissociative excitation of the Lyman-α line as a benchmark. The fact that the measurements were on a relative scale required the establishment of a normalization procedure for merging the low- and high-energy region data sets into a single data volume for analysis. The validity of matching the magnetic and electrostatic data in the region around 200 eV has been confirmed, in a separate experiment, by measuring the Lyman-α signal (normalized to electron beam current and hydrogen source pressure) at 200 eV as a function of a magnetic field, applied collinearly with the *electrostatic gun*, using the same quadrupole magnet configuration employed for the magnetic gun. At field strengths of 0, 20, 40, and 60 G, no statistically significant change in the normalized signal was observed, confirming the absence of any beam overlap problems in the region where the two data sets were merged.

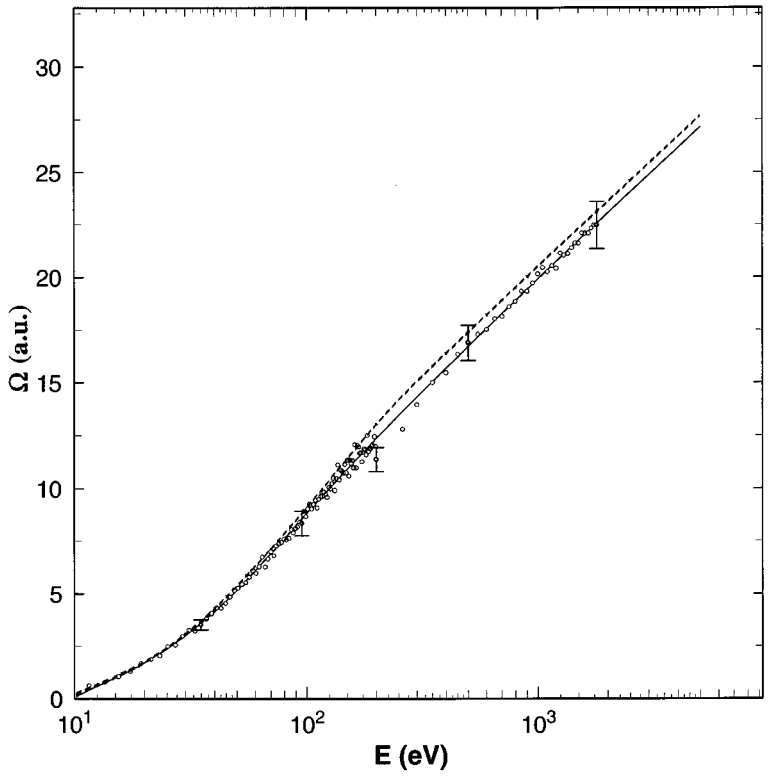

FIG. 9. Experimentally derived collision strength for electron excitation of the H($1s$-$2p$) transition (open circles), compared to an analytic fit to the data using Eq. (10) (solid line), and similar analytic fit to the CCC calculations truncated at 200 eV (dashed line). Representative error bars shown on the figure are estimated combined statistical and systematic uncertainty. Coefficients for the analytic curve are given in Table I.

B. Analytic reduction of data

The data sets were merged by minimizing the root mean square error of the analytic fitting process in the energy region surrounding 200 eV, after the previous corrections for polarization and cascade effects were applied on a relative basis as a correction to the shape function. The fitting process was accomplished using an iterative calculation that established the constant terms in Eq. (10). Figure 9 shows the merged data plotted as collision strength compared to the derived analytic function. The experimental data after corrections described above for cascade and polarization are listed in Table II. The experimental data were placed on an absolute scale determined by fixing the value of C_7 by the known absorption oscillator strength [see Ref. [33], Eq. (9d)]. The higher-order constants C_5 and C_6, two other terms derived from the Born approximation, are not fixed in the analytic fitting process, and therefore the only term fixed in the determination of constants in Eq. (10) is C_7. This matter is discussed further in Sec. V. The constants for Eq. (10) derived in the iterative analytic fit are shown in Table I, along with the Born approximation constants. It is clear that the values of C_5 and C_6, obtained from the fit to the experimental data, do not conform to the Born approximation values. There are, however, large uncertainties in these values, and in the following discussion we conclude that the uncoupled values of the first- and second-order terms of the Born approximation may in any case diverge by large factors from the reality of the coupled system. The data and the analytic curve are plotted in Fig. 9 with representative error bars indicating the calculated level of combined statistical and systematic uncertainty. Comparison of this result with previous measurements described in the Introduction is given in Table III and Fig. 10. The Long *et al.* data [4] are shown as renormalized by vanWyngaarden and Walters [8]. In addition, we have reanalyzed the original Long *et al.* [4] data measured at 90° by correcting for polarization and cascade (in the manner described in Secs. III B and III E), renormalizing to the present cross section at 200 eV.

1. Uncertainty in analytic quantities

Two factors contribute to the uncertainty in determining the experimental cross sections, and in establishing the parameters in the modified Born approximation [Eq. (10)]. First, there is an unusual complexity in the shape of the excitation function. The H($1s$-$2p$) excitation function appears to be unique among atomic cross sections in containing higher-order terms significantly affecting the cross section in the high-energy region. The evidence for this appears in both the present experimental data and CCC calculations. For this reason several parameters share in establishing the magnitude of the cross section in the high-energy region, requiring an unusual range in energy to establish accurate parameter values. Defining the terms in Eq. (10) in the sequence $C_0,\ldots,C_4,C_6,C_5,C_7$ as terms of order $7,\ldots,0$ respectively, we find that terms of order higher than 2 contribute about 50% of the total of terms above the zero order at 500 eV in both the CCC and experimental analysis. In contrast, at the same dimensionless energy ($\sim$50), a similar analysis (Ref. [48]) of the He(^1S-$2\,^1P$) cross section indicates that terms of order higher than 2 contribute only about 1% of total terms above zero order. For this reason the higher-order terms in the case of He are intrinsically more accurately determined. It is only at values of dimensionless energy of $\sim$2 that higher-order terms significantly contribute for the He transition, a factor of 25 in dimensionless energy below the value at which similar effects occur for H. The second component contributing to uncertainty in the analysis is statistical

TABLE II. H($1s$-$2p$) measured electron impact excitation cross sections (a.u.).

E (eV)	$Q_{1s2p}(E)$[a]	$Q_{1s2p}(E)$[b]	E (eV)	$Q_{1s2p}(E)$[a]	$Q_{1s2p}(E)$[b]	E (eV)	$Q_{1s2p}(E)$[a]	$Q_{1s2p}(E)$[b]
1.134+01[c]	3.494−01	3.662−01	9.706+01	6.038−01	6.328−01	1.828+02	4.499−01	4.715−01
1.329+01	3.847−01	4.032−01	9.901+01	5.759−01	6.035−01	1.847+02	4.178−01	4.378−01
1.524+01	4.485−01	4.700−01	1.010+02	5.888−01	6.170−01	1.867+02	4.192−01	4.393−01
1.719+01	4.961−01	5.199−01	1.029+02	5.927−01	6.211−01	1.886+02	4.153−01	4.352−01
1.914+01	5.683−01	5.956−01	1.049+02	5.663−01	5.934−01	1.906+02	4.153−01	4.352−01
2.109+01	5.805−01	6.084−01	1.068+02	5.694−01	5.967−01	1.925+02	4.122−01	4.319−01
2.303+01	5.804−01	6.083−01	1.088+02	5.725−01	6.000−01	1.964+02	4.174−01	4.374−01
2.498+01	6.536−01	6.850−01	1.107+02	5.399−01	5.658−01	1.984+02	3.980−01	4.171−01
2.693+01	6.192−01	6.489−01	1.126+02	5.550−01	5.817−01	2.000+02	3.915−01	4.103−01
2.888+01	6.750−01	7.074−01	1.146+02	5.531−01	5.797−01	2.600+02	3.390−01	3.552−01
3.083+01	6.944−01	7.277−01	1.165+02	5.441−01	5.702−01	3.000+02	3.206−01	3.360−01
3.277+01	6.477−01	6.788−01	1.185+02	5.463−01	5.725−01	3.500+02	2.956−01	3.098−01
3.472+01	6.670−01	6.990−01	1.204+02	5.317−01	5.572−01	4.000+02	2.666−01	2.794−01
3.667+01	6.836−01	7.164−01	1.224+02	5.152−01	5.399−01	4.500+02	2.505−01	2.625−01
3.862+01	6.924−01	7.256−01	1.243+02	5.319−01	5.575−01	5.000+02	2.328−01	2.440−01
4.057+01	7.022−01	7.359−01	1.263+02	5.201−01	5.450−01	5.500+02	2.168−01	2.272−01
4.251+01	6.668−01	6.988−01	1.282+02	5.258−01	5.510−01	6.000+02	2.014−01	2.111−01
4.446+01	6.724−01	7.047−01	1.302+02	5.301−01	5.556−01	6.500+02	1.912−01	2.003−01
4.641+01	6.863−01	7.193−01	1.321+02	4.937−01	5.174−01	7.000+02	1.786−01	1.872−01
4.836+01	7.029−01	7.367−01	1.341+02	5.142−01	5.388−01	7.500+02	1.708−01	1.790−01
5.031+01	6.875−01	7.205−01	1.360+02	5.378−01	5.636−01	8.000+02	1.624−01	1.701−01
5.225+01	6.846−01	7.175−01	1.380+02	4.964−01	5.202−01	8.500+02	1.568−01	1.644−01
5.420+01	6.713−01	7.035−01	1.399+02	5.119−01	5.364−01	9.000+02	1.480−01	1.551−01
5.615+01	6.768−01	7.093−01	1.419+02	5.014−01	5.255−01	9.500+02	1.430−01	1.498−01
5.810+01	6.895−01	7.226−01	1.438+02	4.913−01	5.148−01	1.000+03	1.389−01	1.455−01
6.005+01	6.544−01	6.858−01	1.458+02	5.033−01	5.275−01	1.050+03	1.342−01	1.407−01
6.200+01	6.664−01	6.984−01	1.477+02	4.786−01	5.016−01	1.100+03	1.268−01	1.329−01
6.394+01	6.936−01	7.269−01	1.497+02	4.985−01	5.224−01	1.150+03	1.230−01	1.289−01
6.589+01	6.265−01	6.566−01	1.516+02	4.592−01	4.813−01	1.200+03	1.172−01	1.228−01
6.784+01	6.444−01	6.753−01	1.536+02	4.861−01	5.095−01	1.250+03	1.165−01	1.221−01
6.979+01	6.591−01	6.908−01	1.555+02	4.735−01	4.962−01	1.300+03	1.115−01	1.169−01
7.174+01	6.244−01	6.544−01	1.575+02	4.735−01	4.962−01	1.350+03	1.078−01	1.130−01
7.368+01	6.488−01	6.799−01	1.594+02	4.534−01	4.752−01	1.400+03	1.053−01	1.104−01
7.563+01	6.414−01	6.722−01	1.614+02	4.924−01	5.160−01	1.450+03	1.027−01	1.076−01
7.758+01	6.308−01	6.611−01	1.633+02	4.425−01	4.637−01	1.500+03	9.920−02	1.040−01
7.953+01	6.282−01	6.584−01	1.652+02	4.795−01	5.025−01	1.550+03	9.820−02	1.029−01
8.148+01	6.104−01	6.397−01	1.672+02	4.716−01	4.942−01	1.600+03	9.506−02	9.962−02
8.342+01	6.015−01	6.304−01	1.691+02	4.542−01	4.760−01	1.650+03	9.220−02	9.662−02
8.537+01	6.188−01	6.485−01	1.711+02	4.496−01	4.712−01	1.700+03	9.049−02	9.484−02
8.732+01	5.943−01	6.228−01	1.730+02	4.286−01	4.492−01	1.750+03	8.849−02	9.274−02
8.927+01	5.969−01	6.255−01	1.750+02	4.394−01	4.604−01	1.800+03	8.598−02	9.011−02
9.122+01	5.894−01	6.176−01	1.769+02	4.419−01	4.631−01			
9.316+01	5.936−01	6.221−01	1.789+02	4.355−01	4.564−01			
9.511+01	5.767−01	6.044−01	1.808+02	4.223−01	4.426−01			

[a]Present measured cross section, corrected and scaled using analytic fit, as discussed in text.

[b]Present measured cross section, normalized using Bethe-Fano plot as described by Ref. [11]. These values are likely to be the upper limit of the true cross section.

[c]Read as 1.134×10^{1}.

and systematic errors in the measurements, generally less than 4%, as discussed in the Appendix.

The estimated 10% uncertainty in the present experimental result, therefore, stems primarily from the heavy mixing of the higher-order terms in the analytic fit to the data. The uncertainty in the values of the first- and second-order terms in the analyzed experiment is large enough to encompass the values for these terms in the Born approximation, and therefore the terms are poorly constrained. The role played by the uniqueness of the shape function is illustrated by the variance of the coefficients in fitting the CCC calculations, as shown in Table I. The analysis restricted to the energy range

TABLE III. H($1s$-$2p$) selected experimental electron impact excitation cross sections (a.u.).

E (eV)	$Q_{1s2p}(E)$		
11.0	0.192[a]		0.212[e]
13.4	0.413	0.42[b]	0.332
16.0	0.506	0.50	0.424
18.5	0.553	0.55	0.473
23.5	0.609	0.65	0.570
28.5	0.643	0.70	0.624
38.6	0.678	0.72	0.658
48.6	0.683	0.72	0.650
54.4	0.678	0.888[c]	
68.6	0.654	0.68[b]	0.623
88.7	0.608	0.64	0.578
118.8	0.540	0.56	0.505
148.9	0.482	0.52	0.466
200.0	0.409	0.45	0.409
1000.0	0.138	0.135[d]	
1200.0	0.119	0.126	
1400.0	0.105	0.109	
1600.0	0.095	0.099	
2000.0	0.079	0.086	

[a]Analytic fit to present experiment.
[b]van Wyngaarden and Walters [8] reanalysis of Ref. [4] experiment; see text.
[c]Williams [7].
[d]Schartner [53].
[e]Present reanalysis of Ref. [4] experiment; see text.

up to 2 keV shown in the fifth column of Table I produces an error of 7% in returning the value of the zero-order term, utilizing data considered to be internally accurate to 1%. The difficulty in establishing accurate values of the higher-order terms is discussed further in the examination of the CCC calculations.

2. Conventional normalization using a Bethe-Fano plot

A conventional normalization procedure was also applied to the experimental data in the manner described in detail by Heddle and Gallagher [11]. In this approach, the experimental collision strength data are first corrected for polarization and cascade, and then placed on an absolute scale by fitting to the asymptotic Born limit at high energy defined by a Bethe-Fano line. The formulation for this line described by [11] is equivalent to Eq. (9a) but without the C_6 term. The slope (determined from the constant C_7) is related to the known optical oscillator strength [Eqs. (8b), (8c)] and the energy intercept is fixed using the Born value of C_5 [Eq. (9b)]. On a plot of collision strength (using the units of cm^2 eV) vs $\log[E(\mathrm{eV})]$, the resulting Bethe-Fano line has a slope of 6.129×10^{-15} cm^2 eV and an energy intercept at 8.337 eV [11].

A fit of the experimental data to this Bethe-Fano line over the energy range 1–1.8 keV is shown in Fig. 11. The resulting values for the H($1s$-$2p$) excitation cross section are listed in Table II. These data lie approximately 4.8% above the values obtained using the analytic fitting procedure [Eq. (10)] and thus agree more closely with the CCC calculations.

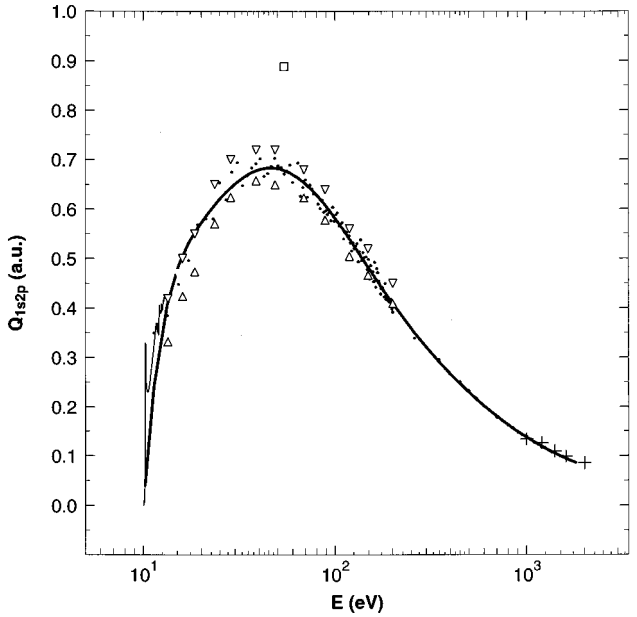

FIG. 10. Summary plot of experimental H($1s$-$2p$) cross sections. Dots: present work normalized using analytic fit described in Sec. IV; thick line: analytic fit to present data set; thin line: Williams [6] near threshold data; open square: Williams [7]; up triangle: Long *et al.* [4] data corrected for polarization (using Ref. [9]) and cascade (using present model [31]) then normalized to present cross section at 200 eV; down triangle: Long *et al.* [4] data corrected by van Wyngaarden and Walters [8] for polarization and cascade and normalized to their theoretical value at 200 eV; pluses: Schartner [53].

The agreement with CCC theory is within 3% over the entire energy range of the experiment, as shown in Fig. 12. At the critical energy of 54.4 eV, for example, the experimental H($1s$-$2p$) cross section derived using the Bethe-Fano normalization approach is 0.710 a.u., compared to the CCC value of 0.729 a.u. and a value of 0.708 a.u. quoted in the

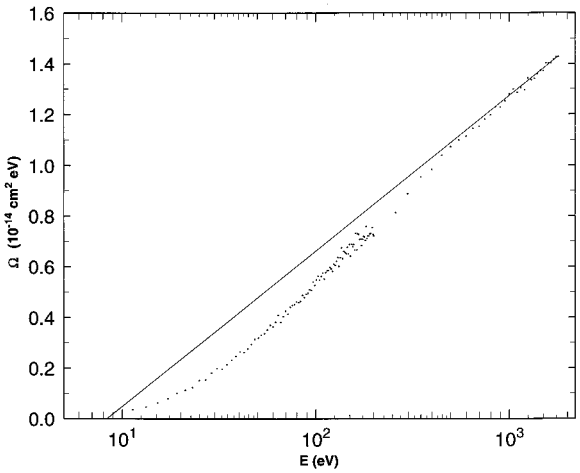

FIG. 11. Experimental H($1s$-$2p$) collision strength data (dots) normalized by fitting to a Bethe-Fano line (solid) in the high-energy region from 1 keV to 1.8 keV in the manner described by Heddle and Gallagher [11]. The slope and intercept of the Bethe-Fano line are defined by Born constants.

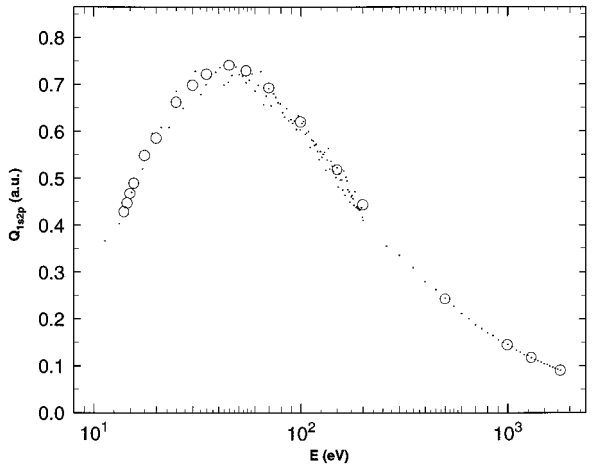

FIG. 12. Experimental H($1s$-$2p$) cross section (dots) derived from a conventional Bethe-Fano normalization procedure compared to the theoretical CCC calculations (open circles). The experimental cross section values and the CCC values above 500 eV are likely to be an upper limit to the true cross section.

van Wyngaarden and Walters [8] analysis of the Long *et al.* data [4]. The better agreement of this result with the CCC calculations above 1 keV is due to the fact that the CCC calculations converge on the Born value for the first-order (C_5) term. The Bethe-Fano line method used here (Fig. 11) did not rely on the data to determine the intercept since in this case it is defined by the Born value of C_5. If, however, the Bethe-Fano line is defined by an optimum fit of the data above 1 keV, we find a value $C_5=-0.5$, substantially below the Born value of 0.8988, but similar to the value (-0.29) derived from the analysis described above. This results in a cross section consistent with the analytic fit to the entire data set described above in this section.

C. Theoretical calculations

The literature is replete with calculated cross sections for the H($1s$-$2p$) transition. It is not the intent of this paper to review the merits of these published results. We refer the reader to the recent review in Ref. [1]. Considerations here

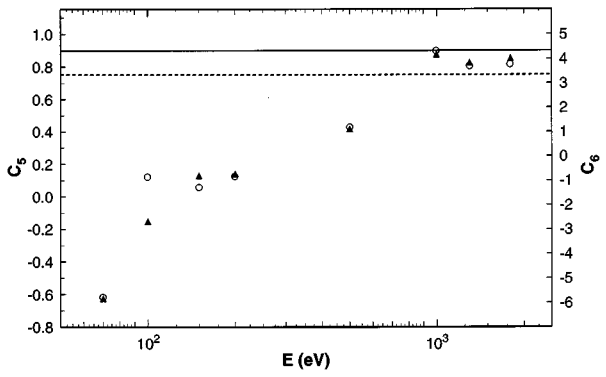

FIG. 13. The variation of the first- (C_5, open circles) and second- (C_6, triangles) order coefficients of the analytic function Eq. (10), fitted to the CCC calculations truncated at the energies indicated on the abscissa. In the ideal case the coefficients should be invariant on this plot. The Born values of C_5 and C_6 are indicated by the solid and dashed lines, respectively.

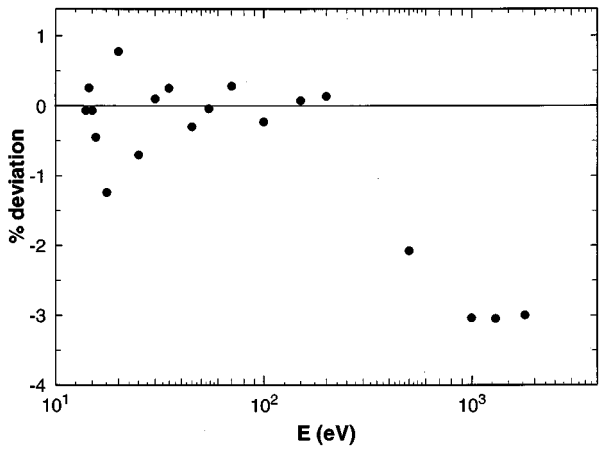

FIG. 14. Deviation of analytic model, Eq. (10), from CCC calculations of the H($1s$-$2p$) collision strength. The analytic model fit was limited to 200 eV in the CCC data. The plotted points are the percentage deviation calculated after subtracting the CCC calculations from the model values.

are restricted to calculated cross sections in the work by Byron *et al.* [25], Bubelev *et al.* [17], and the present CCC calculations. The work by Byron, Joachain, and Potvliege [25] is a unitarized eikonal Born series calculation that provides a useful comparison with the more recent DWBA2 [17] and CCC methodologies. The latter results are of critical interest because of their expected high accuracy [19]. The analysis of these calculations by fitting the results analytically using Eq. (10) indicates that the effects of multistate coupling extend significant influence on the shape function to energy in the range up to 1 keV. This introduces significant systematic uncertainty in the separation of the coefficients, as discussed above. The effect appears within the theoretical calculations, presenting uncertainty in determination of the values of the coefficients that should be used as an appropriate representation of the theory. For this reason we discuss the determination of the coefficients in more detail here.

1. Analysis of the CCC calculations

Table I (fifth column) shows the coefficients derived in fitting Eq. (10) to the CCC calculations up to 2 keV, allowing all coefficients to be freely determined. As we have noted this results in a value of C_7, 7% larger than the Coulomb (Born) approximation (cf. Ref. [32]). Due to the fact that the optical oscillator strength [which determines C_7 in Eq. (8b)] is, however, a quantity internalized in the nonperturbative CCC calculation, the result represents uncertainty in the fitting process caused by the heavy mixing of the terms in energy space. A more satisfactory result is obtained by fixing the value of the zero-order constant to that given by Eq. (9d). We find in analyzing the CCC calculations in this way that the values of the higher-order terms vary systematically, depending on the value of the upper energy limit at which the data set is terminated. In principle, the values of the constants should be independent of the data termination point. In fact, the derived values of the first- and second-order constants in this case show a systematic downward trend in real numeric value, as a function of decreasing truncation energy, as shown in Fig. 13. The implication of the variation in Fig.

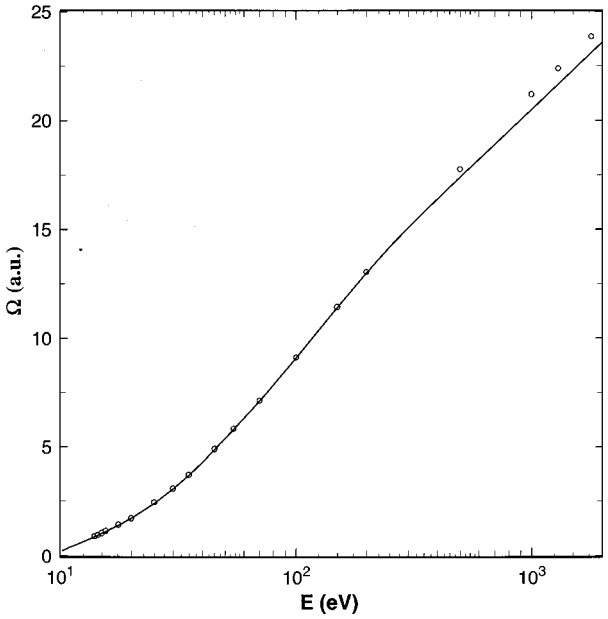

FIG. 15. Recommended H($1s$-$2p$) analytic electron collision strength (see text) derived from the CCC calculations (solid line) by fitting with Eq. (10) from 14 to 200 eV, compared to the calculated CCC values (open circles).

13 is that the generalized oscillator strength implied from the CCC calculation is somewhat unstable in shape. From a number of repeated calculations of various sizes, we estimate that at intermediate energies ($\sim$50 eV) the CCC cross section values are within 3% of reality at the 90% confidence level, and at 1 keV, 5% at the 90% confidence level. The decreasing accuracy in the calculation toward higher energy is attributed to increasing amounts of oscillations in numerical integrations. We use this estimate of accuracy in the calculation as a basis for choosing the energy range most suitable for deriving the Eq. (10) term constants. In this case we select the coefficients established in fitting the CCC data up to 200 eV as the most accurate representation of the function. Table I (fourth column) shows the derived constants for this case, considered here to be the optimal fit to the CCC calculation. Figure 14 shows the percentage deviation of the fitted curve from the CCC collision strengths. We note that the analytic function falls systematically below the CCC values at electron energies above 200 eV, deviating by about 3.6% at 1 keV. The analytic fit also falls below the Born approximation in the 1 keV region, conforming with the general tendency of Born cross sections to be larger than reality (Refs. [29,49], Fig. 1). The analytic fit and the CCC collision strength values are compared in Fig. 15.

2. Comparison of cross sections

Although the DWBA2 and CCC calculations are not explicitly constrained at high energies by the Born approximation, they tend to converge on the Born values near 1 keV (see Fig. 1). The fact that the two higher-order terms in Eq. (9a) depend on the shape of the generalized oscillator strength indicates that the values of these terms in the Born approximation should deviate from reality in cases in which the cross section is significantly affected by interstate coupling. A computational method known as ''Born subtraction'' has been utilized in these theoretical calculations at all energies, which allows the treatment of the partial-wave expansion to infinity. The CCC and DWBA2 calculations do not accurately constrain the first- and second-order terms, because a 1% error in the calculation at 1 keV translates into a large uncertainty in the higher-order term values. The implication is that a systematic or statistical uncertainty in the calculated cross section at the level of 1% can produce an error of order 10% in the oscillator strength derived from the theoretical result, caused primarily by the encroachment of multistate coupling effects into the 1 keV region of the excitation function.

The cross sections are compared numerically in Table IV. It can be seen that the analytic fit to the experimental data falls below the CCC data by between 3% and 7% over the 2 keV energy band except near threshold. The most remarkable aspect of the comparison of the CCC calculations and the analytic results derived from the current experimental data is the similarity of the shape functions. The difference in shape is most easily observed in Fig. 9, where the analytic fits to the CCC and experimental data are plotted in the form of collision strengths. The most significant difference appears in the 60–500 eV region where the magnitude of the difference is near the limit of experimental uncertainty. This region in electron energy is, however, the most vulnerable region for errors to occur in the present experiment.

Table IV includes the DWBA2 calculations of Ref. [17] and UEBS results from Ref. [25]. The DWBA2 cross sections are significantly larger than the CCC, UEBS, and the present experimental results at and below 150 eV (see Fig. 1). The analysis of the present experimental results are within 3% of the UEBS Ref. [25] calculations (Table IV).

V. DISCUSSION AND CONCLUSIONS

The most important consideration in the comparison of the experimental data with the theoretical results is the shape of the excitation function. We find, as shown in Sec. IV, that the shape of the analyzed experimental data conforms to the CCC calculations, within estimated uncertainty (see Fig. 9). The analysis of both the experiment and the CCC theory using a modified analytic Born approximation, described in Sec. IV, indicates that higher-order terms influence the cross section to an unusually high energy. The effect of this is to increase the uncertainty in the experimental absolute cross section derived from the analytic fit to an estimated 10%, while statistical and systematic uncertainties were limited to 2–4 %. A similar analysis of the CCC calculations setting an upper bound in energy at the same level as the experimental data produced a similar error (in the opposite direction) in the value of the derived optical oscillator strength (Table I). This is a clear indication that the accuracy of this or any other methodology is limited for H($1s$-$2p$) primarily by the subtle changes in shape function reaching into the high-energy region. The unique nature of the shape is presumed to be caused primarily by the strong coupling of the $2s$ and $2p$ states.

The difficulty in separating the terms above zero order is illustrated in the analysis of the CCC calculations shown in Fig. 13. This figure shows the variation in the first- and

TABLE IV. H($1s$-$2p$): Comparison of electron impact excitation cross sections (a.u.).

E (eV)	$Q_{1s2p}(E)$					
1.40+01[a]	4.28−01[b]	4.26−01[c]				4.42-01[d]
1.45+01	4.47−01	4.48−01				4.62−01
1.50+01	4.67−01	4.67−01	8.34−01[e]			4.79−01
1.56+01	4.89−01	4.87−01				4.96−01
1.76+01	5.48−01	5.41−01				5.38−01
2.00+01	5.85−01	5.89−01	8.78−01			5.73−01
2.50+01	6.62−01	6.57−01	8.99−01			6.21−01
3.00+01	6.98−01	6.99−01				6.51−01
3.50+01	7.21−01	7.23−01				6.70−01
4.50+01	7.40−01	7.38−01				6.83−01
5.44+01	7.29−01	7.29−01	8.46−01		7.10−01[f]	6.78−01
7.00+01	6.92−01	6.94−01	7.84−01			6.51−01
1.00+02	6.20−01	6.19−01	6.76−01	6.04−01[g]		5.81−01
1.50+02	5.18−01	5.18−01	5.46−01			4.80−01
2.00+02	4.43−01	4.44−01	4.59−01	4.14−01		4.09−01
3.00+02		3.42−01		3.02−01	3.36−01	3.20−01
4.00+02		2.79−01		2.60−01	2.79−01	2.67−01
5.00+02	2.42−01	2.37−01	2.42−01		2.44−01	2.30−01
9.99+02	1.44−01	1.40−01	1.43−01		1.45−01	1.38−01
1.30+03	1.17−01	1.13−01			1.17−01	1.12−01
1.80+03	9.01−02	8.74−02			9.01−02	8.61−02
2.00+03		8.02−02				7.91−02
3.00+03		5.76−02				5.68−02
4.00+03		4.54−02				4.47−02
5.00+03		3.76−02				3.71−02
6.00+03		3.23−02				3.19−02
7.00+03		2.83−02				2.80−02
8.00+03		2.53−02				2.50−02
9.00+03		2.29−02				2.26−02
1.00+04		2.09−02				2.06−02

[a]Read as 1.4×10^{1}.
[b]CCC method.
[c]Analytic fit to CCC data to 200 eV, Eq. (10).
[d]Analytic fit to present experimental data; see text.
[e]DWBA2 method; Ref. [17].
[f]Present experimental data, normalized using Bethe-Fano plot as described by [11]. These values are likely to be the upper limit of the true cross section. Value at 54.4 eV is interpolated.
[g]UEBS method; Ref. [25].

second-order terms in the analysis of the CCC data as a function of the energy of the upper truncation point in the analyzed data set. One can see from the figure that the C_5 and C_6 values are close to the values of the Born approximation constants (Table I) for truncation energies at or above 1 keV. At 500 eV (Fig. 13), however, the values of the constants suddenly drop in the optimal fitting process by factors of about 2 and 4. The uncertainty in the coefficients derived from the experimental data is at least this large. At lower energies the real numeric values of the constants continue to decline systematically in the analysis of the CCC calculations, as shown in Fig. 13. In principle the constants should be invariant. Although the form of the analytic formulation may play a small role in defining this variation, very small computation errors within the stated uncertainty of the CCC calculations can easily be responsible for the behavior shown in Fig. 13.

The accuracy of the analytic fit to the CCC data is shown for the selected case in Fig. 14 where the maximum deviation in the fit is 3.3% at 1 keV, and generally in the range less than 0.5% at energies below 500 eV. We select the constants in the analytic terms for the fit to the CCC calculations for an upper truncation energy of 200 eV as the recommended representation of the CCC cross section (Table I, fourth column). This produces cross sections that fall below the Born approximation at energies in the 1 keV range, by about 3%, consistent with the argument that the higher-order constants in the Born approximation are upper limits to the coupled system constants (Refs. [29,49]; see Fig. 1). The collision strengths derived from the CCC and the experimental results are compared in Fig. 9. The numeric values of the cross sections are compared in Table IV.

We summarize our conclusions with the following points.

(1) We conclude, based on the consideration of the com-

TABLE V. Recommended electron impact H($1s$-$2p$) excitation cross sections (a.u.).

E (eV)	$Q_{1s2p}(E)$	E (eV)	$Q_{1s2p}(E)$	E (eV)	$Q_{1s2p}(E)$
1.50+01[a]	4.667−01[b]	2.65+01	6.720−01	1.00+02	6.186−01
1.52+01	4.737−01	2.70+01	6.764−01	1.10+02	5.959−01
1.54+01	4.804−01	2.80+01	6.846−01	1.20+02	5.747−01
1.56+01	4.868−01	2.90+01	6.920−01	1.30+02	5.548−01
1.58+01	4.931−01	3.00+01	6.987−01	1.40+02	5.360−01
1.60+01	4.991−01	3.10+01	7.048−01	1.50+02	5.184−01
1.62+01	5.050−01	3.20+01	7.101−01	1.60+02	5.018−01
1.64+01	5.106−01	3.30+01	7.149−01	1.70+02	4.860−01
1.66+01	5.161−01	3.40+01	7.192−01	1.80+02	4.711−01
1.68+01	5.214−01	3.50+01	7.229−01	1.90+02	4.570−01
1.70+01	5.266−01	3.60+01	7.261−01	2.00+02	4.436−01
1.72+01	5.316−01	3.70+01	7.289−01	2.50+02	3.864−01
1.74+01	5.365−01	3.80+01	7.312−01	3.00+02	3.421−01
1.76+01	5.412−01	3.90+01	7.332−01	3.50+02	3.072−01
1.78+01	5.458−01	4.00+01	7.347−01	4.00+02	2.792−01
1.80+01	5.503−01	4.10+01	7.360−01	4.50+02	2.562−01
1.92+01	5.750−01	4.20+01	7.369−01	5.00+02	2.370−01
1.94+01	5.788−01	4.30+01	7.375−01	5.50+02	2.207−01
1.96+01	5.825−01	4.40+01	7.378−01	6.00+02	2.067−01
1.98+01	5.861−01	4.50+01	7.378−01	7.00+02	1.839−01
2.00+01	5.896−01	4.60+01	7.377−01	8.00+02	1.660−01
2.05+01	5.980−01	4.70+01	7.372−01	9.00+02	1.515−01
2.10+01	6.060−01	4.80+01	7.366−01	1.00+03	1.395−01
2.15+01	6.136−01	4.90+01	7.358−01	1.20+03	1.209−01
2.20+01	6.209−01	5.00+01	7.348−01	1.40+03	1.069−01
2.25+01	6.277−01	5.44+01	7.287−01	1.60+03	9.610−02
2.30+01	6.342−01	6.00+01	7.179−01	1.80+03	8.740−02
2.35+01	6.404−01	6.50+01	7.064−01	2.00+03	8.026−02
2.40+01	6.464−01	7.00+01	6.940−01	2.50+03	6.691−02
2.45+01	6.520−01	7.50+01	6.811−01	3.00+03	5.760−02
2.50+01	6.574−01	8.00+01	6.682−01	3.50+03	5.070−02
2.55+01	6.625−01	8.50+01	6.554−01	4.00+03	4.538−02
2.60+01	6.674−01	9.00+01	6.428−01	4.50+03	4.113−02
		9.50+01	6.305−01	5.00+03	3.765−02

[a]Read as 1.50×10^{1}.

[b]Recommended cross section (a.u.), from analytic fit to the present CCC theory. See Table I, fourth column, for analytic coefficients.

bined effects, that the accuracy of the absolute cross section derived from the experimental measurements reported here for the H($1s$-$2p$) transition are limited to about 10%.

(2) The strong coupling of states, evident in the analysis of both the theoretical and experimental results, suggests that the shape of the generalized oscillator strength deviates significantly from the Born ($1s$-$2p$) shape function [Eq. (7)]. The first- and second-order terms in the modified Born approximation are therefore expected to deviate substantially from the uncoupled Born values. The experimental and theoretical CCC results, however, do not put strong constraints on the values for the coefficients of these terms, implying uncertainty in the exact shape of the generalized oscillator strength. The first-order constant derived from the experiment and analysis of the CCC calculations is substantially smaller than the uncoupled Born value. The analytic fit to the experimental data described in Sec. IV produces a smaller cross section than either the present CCC calculations or the uncoupled Born approximation, because the derived value of the first-order constant, C_5, is significantly below the Born value. Analysis of the experimental data above 1 keV using the Bethe-Fano line method, in which C_5 is determined by optimal fit to the data, also produces a significantly smaller value, indicating that the experimental data is internally consistent over the whole range of energy. The sense of the discrepancy with the first-order Born constant is also consistent with the effect of coupling on the values of those terms affected by momentum transfer in the collision process. The analysis of the experimental and CCC cross sections depends on the knowledge of the optical oscillator strength for the H($1s$-$2p$) transition. It has been assumed that the value of this constant is unaffected by coupling effects. Given the strength of the ($2s$-$2p$) coupling for the e-H system, and hence its effect on the ($1s$-$2p$) channel, analysis of the cross section is particularly difficult.

(3) Since the present measurements are consistent with

the CCC calculations, within stated error bars, we recommend that the analytic coefficients derived from the CCC results given in Table I, fourth column, be utilized as a cross section model for electron impact energies from 15 eV to 5 keV. For astrophysical model applications, there is no practical difference between the present experiment and the CCC results. Table V lists values of the recommended cross section for selected energies. Resonance and exchange effects, not determined here, must be included to define the cross section to near threshold energies. The near threshold H($1s$-$2p$) cross section and a model of the general discrete atomic hydrogen emission properties [H(nl-$n'l'$)] will be given in a future paper (Ref. [31]).

ACKNOWLEDGMENTS

This work was carried out at the Jet Propulsion Laboratory, California Institute of Technology, and the University of Southern California. The work at the Jet Propulsion Laboratory was supported by the Atomic, Molecular and Optical Physics program of the National Science Foundation (Grant No. PHY-9220742), the Astrophysics and Planetary Atmospheres programs of the National Aeronautics and Space Administration, and by the Air Force Office of Scientific Research. The work at the University of Southern California was supported by the National Science Foundation (Grant No. ATM-9320589) and NASA (Grant No. NAGW-3905). J. W. M. acknowledges support from the Natural Sciences and Engineering Research Council of Canada. In addition, we gratefully acknowledge Don Madison and Vladimir Bubelev for providing us with their DWBA2 calculations, James Walters for supplying us with the results of his first Born calculation, and Bill Ott for providing digital values of his polarization measurements. The authors also wish to acknowledge Bill Lanigan for his invaluable assistance in the design and implementation of the computer control of the experimental apparatus, and Sandor Trajmar for critical comments on the manuscript.

APPENDIX: ANALYSIS OF EXPERIMENTAL ERRORS

A comprehensive analysis of statistical and systematic errors was performed in order to determine the accuracy of the present measurements. The additional factors involved in establishing absolute values from the analytic fit to the data are discussed in Sec. IV. Sources of error in the measured signal are detailed below.

(1) *Variations in electron beam current and hydrogen source pressure:* The experimental system is interfaced to a PC-based data acquisition and control system which monitors critical parameters of our experiment and normalizes the measured signals to the electron beam current and hydrogen source pressure, eliminating known sources of systematic error. Data are accumulated in a multiple scanning mode to reduce the effects of drift in other experimental parameters.

(2) *The measured dissociation fraction:* Since the dissociation fraction (D) is needed for subtraction of the molecular Lyman-α contribution to the observed signal, there is an uncertainty in the derived atomic signal produced by the error in the measured value of D. Measurement of the dissociation fraction has a relative error of $\sim\pm 3\%$, based on the signal statistics of the discharge on and off measurements performed at 110.0 nm. For a (typical) dissociation fraction of 0.65, this produces a net error in the molecular subtraction procedure of $\pm 0.2\%$ for the electrostatic gun data, and of $\sim\pm 1\%$ for the magnetic gun data, reflecting the lower accumulated signal of the latter. The accuracy of the molecular subtraction procedure is demonstrated in Fig. 6.

(3) *Composition of the partially dissociated H-H_2 beam.* There are a number of possible systematic effects related to the use of the rf discharge H source that Rudd *et al.* [50] suggest could lead to compositional or density variations in the H or H_2 species produced. These possible effects have been identified and eliminated as sources of any significant systematic error in the present work, as follows. (a) Different kinetic temperatures in the gas beam with the discharge on or off. Efficient wall thermalization as the beam exits the discharge tube has been clearly demonstrated by Woolsey *et al.* [44] and Forand *et al.* [43] in an identical source. (b) H($2p$) production could occur from some other long-lived atomic species such as H($2s$) or H(Rydberg). Again, Forand *et al.* [43] have demonstrated that these were not a problem by introducing quench fields which had no effect on observed signals. Furthermore, if any such excitation was occurring, a change in the observed threshold would have been observed (i.e., signal would have been observed below 10.2 eV). (c) Excitation of H($2p$) or H_2 could occur for some long-lived electronically excited molecular species. This can be discounted for the reasons given under (b) above. (d) Vibrationally excited H_2 could be present in the beam and this could perturb the measurement of the dissociation fraction because of the different Franck-Condon factors involved. Again, this was considered by Forand *et al.* [43] and can be discounted since (i) the effective temperature of the exit nozzle of the source is low so the molecules are effectively thermalized to $v=0$, and (ii) if significant population of states other than $v=0$ was occurring then the vibrational distribution observed in emission after the electron impact process would be quite different from the distribution seen with the discharge off. Thus the subtraction procedure would not yield the flat backgrounds that are observed in Fig. 6. In addition, a significant amount of vibrational excitation would also have affected the threshold. It should be noted that the dissociation fractions measured in the present work are consistent with those measured by other experimenters using this type of rf source, where mass spectrometers have been used to determine the dissociation fraction.

(4) *Statistical errors in the observed signal count rates:* The statistical error (assuming a Poisson distribution) in the net signal varies since the signal flux changes with energy and is also different for the electrostatic and magnetic gun configurations. For the electrostatic gun, the signal statistics varied from $\pm 0.3\%$ at 200 eV to $\pm 0.6\%$ at 1.8 keV. For the magnetic gun data, the statistical errors varied from $\pm 3.2\%$ near threshold to $\pm 2.6\%$ at 200 eV.

(5) *Error in the polarization correction.* Since the signal flux obtained at 90° must be corrected by the factor $(1-P/3)$ in order to derive the total cross section, an error is introduced from the uncertainty in the polarization P. Polarization data for H Lyman-α measured by Ott *et al.* [9] have reported absolute error bars of ± 0.01 or less in the region from threshold to 200 eV. This results in a relative error of

up to $\pm 0.3\%$ in the polarization correction procedure. For energies above 200 eV, the McFarlane formulation [41] [Eq. (11)] for the polarization was used. Although a realistic estimate of the error in the McFarlane approach is not possible, the polarization fractions are, in any case, relatively small in this energy region (maximum ~ 0.1), and the resulting error can be safely taken to be negligibly small.

(6) *Detector background subtraction:* The detector background noise subtraction is particularly important at the highest electron impact energies where the signal strength is lowest and the accuracy of the normalization procedure is critically dependent on the quality of the experimental data. This background was measured to an accuracy of $\pm 2\%$, which results in an error of up to $\sim \pm 0.2\%$ in the determination of the atomic signal at the highest energy.

(7) *Quenching of H(2s):* Deactivation of $2s$ metastable atoms into the $2p$ state within the field of view of the detector would introduce an erroneous component to the signal. The interaction region was, however, rigorously shielded to ensure the absence of stray fields. In the case of possible fringing fields from the biasing voltages applied to the Faraday cup, a systematic investigation of the Lyman-α signal, as a function of these voltages, revealed no statistically significant dependence on stray fields from this source. We conclude that there is no significant contribution to the signal arising from quenching of the $2s$ metastable population by field effects. The electron beam, in addition to exciting the $2s$ state, also deactivates the $2s$ into the $2p$ state with a collision strength of about 600 a.u. (see Purcell [51]). The maximum beam current in this experiment is 18 μA at 12 eV, corresponding to a deactivation time of about 2 msec. Electron collisions therefore dominate the deactivation process. The effect, however, is negligible in this case because of the very short lifetime of the H atoms in the beam compared to the production and deactivation lifetimes. The steady state model calculations determining the cascade contribution were for this reason carried out neglecting the $(2s\text{-}2p)$ collisional transition (see [31]).

(8) *Errors associated with magnetic field confinement of the electron beam:* The use of magnetic confinement to produce the electron beam can lead to errors arising from energy dependent path length differences in the interaction region due to the helical trajectories of the electrons. At very high electron densities there is also the possibility of nonlinearities in the beam profile due to space charge induced scalloping of the beam. Using the correction factors described by Taylor *et al.* [52] we estimate that path length variations of our electron beam are not significant at energies up to 200 eV used in the present experiment. In the case of scalloping, we were careful to use electron currents well below the space charge limit at each energy. We believe that any effects associated with magnetic field confinement are not significant in the present experiment. Indeed, the similarity between the shapes of the renormalized excitation function data of Long *et al.* [4] shown in Fig. 10 and the present work adds additional confidence to this claim since the Long *et al.* [4] data from threshold to 200 eV were obtained with an electrostatic gun in the absence of any magnetic field.

(9) *Errors associated with low-energy secondary electrons:* Historically, excitation function measurements have been plagued by problems associated with the presence of secondary electrons in the interaction region. These electrons can cause further excitation, leading to erroneous signals, especially in the critical high-energy region where data are normalized and where a relatively small secondary component can lead to a disproportionately large contribution to the atomic signal. Secondary electrons are a particular problem for magnetic guns, where electrons produced in ionizing collisions and at gun apertures can be trapped in the confining magnetic field. The selection of an electrostatic gun for the energy region above 200 eV ensures the absence of any magnetically trapped secondary electrons. It should also be noted that we could not get acceptable convergence of our data at high energies to the Born limit using our magnetic gun.

(10) *Error in the cascade correction:* This is a difficult error to quantify since our cascade corrections depend on the accuracy of various theoretical calculations, as described in Sec. III E. The magnitude of the cascade correction is highly dependent on energy, decreasing from a $\sim 27\%$ correction near threshold to $\sim 3\%$ at 1.8 keV. It has been pointed out by Van Zyl and Gealy [46] that small electric fields can significantly perturb the cascade contribution. Errors in cascade corrections can be a significant factor in the accuracy of our Q_{1s2p} data, especially at energies below 40 eV, where the corrections are large. In presenting our data, we have assumed an uncertainty of $\pm 10\%$ in the cascade corrections at all energies.

The above errors are combined appropriately in quadrature to obtain values for the total experimental error in (a) the measured Lyman-α signal and (b) the derived relative Q_{1s2p} values. For the electrostatic gun data, the resulting calculated error in (a) increases from $\pm 0.3\%$ at 200 eV to $\pm 1.8\%$ at 1.8 keV. The corresponding errors in (b) are $\pm 0.5\%$ and $\pm 1.9\%$, respectively. For the magnetic gun data, the error in (a) is $\sim \pm 3.4\%$ near threshold, reducing to $\pm 2.8\%$ at 200 eV. The corresponding errors in (b) are $\sim \pm 4\%$ near threshold, reducing to $\sim \pm 2.9\%$ at 200 eV.

The analytic fitting of the experimental data using Eq. (10) reduces the statistical contribution to the uncertainty in data values to a negligible contribution relative to the systematic errors. The effect of the systematic factors is discussed in Sec. IV.

[1] S. Trajmar and I. Kanik, in *Atomic and Molecular Processes in Fusion Edge Plasmas*, edited by R. K. Janev (Plenum, New York, 1995), p. 31.

[2] G. C. King, S. Trajmar, and J. W. McConkey, Comments At. Mol. Phys. **23**, 229 (1989).

[3] W. L. Fite and R. T. Brackmann, Phys. Rev. **112**, 1151 (1958).

[4] R. L. Long, D. M. Cox, and S. J. Smith, J. Res. Natl. Bur. Stand. Sect. A **72A**, 521 (1968).

[5] J. W. McGowan, J. F. Williams, and E. K. Curley, Phys. Rev. **180**, 132 (1969).

[6] J. F. Williams, J. Phys. B **9**, 1519 (1976).
[7] J. F. Williams, J. Phys. B **14**, 1197 (1981).
[8] W. L. van Wyngaarden and H. R. J. Walters, J. Phys. B **19**, L53 (1986).
[9] W. R. Ott, W. E. Kauppila, and W. L. Fite, Phys. Rev. A **1**, 1089 (1970).
[10] D. J. T. Morrison and M. R. H. Rudge, Proc. Phys. Soc. London **89**, 45 (1966).
[11] D. W. O. Heddle and J. W. Gallagher, Rev. Mod. Phys. **61**, 221 (1989).
[12] L. A. Vainshtein, Opt. Spektrosk. **18**, 947 (1965) [Opt. Spectrosc. (USSR) **18**, 538 (1965)].
[13] U. Fano, Phys. Rev. **95**, 1198 (1954).
[14] D. H. Madison, Comments At. Mol. Phys. **26**, 59 (1991).
[15] P. J. M. van der Burgt, W. B. Westerveld, and J. S. Risley, J. Phys. Chem. Ref. Data **18**, 1757 (1989).
[16] D. E. Shemansky, J. M. Ajello, and D. T. Hall, Astrophys. J. **296**, 765 (1985).
[17] V. E. Bubelev, D. H. Madison, I. Bray, and A. T. Stelbovics, J. Phys. B **28**, 4619 (1995).
[18] P. G. Burke, K. A. Berrington, and C. V. Sukumar, J. Phys. B **14**, 289 (1981).
[19] I. Bray and A. T. Stelbovics, Phys. Rev. A **46**, 6995 (1992).
[20] I. Bray and A. T. Stelbovics, Adv. At. Mol. Phys. **35**, 209 (1995).
[21] J. Callaway and K. Unnikrishnan, Phys. Rev. A **48**, 4292 (1993).
[22] W. L. van Wyngaarden and H. R. J. Walters, J. Phys. B **19**, 929 (1986).
[23] M. P. Scott, T. T. Scholz, H. R. J. Walters, and P. G. Burke, J. Phys. B **22**, 3055 (1989).
[24] A. E. Kingston and H. R. J. Walters, J. Phys. B **13**, 4643 (1980).
[25] F. W. Byron, Jr., C. J. Joachain, and R. M. Potvliege, J. Phys. B **18**, 1637 (1985).
[26] A. R. Filipelli, C. C. Lin, L. W. Anderson, and J. W. McConkey, Adv. At. Mol. Phys. **33**, 1 (1994).
[27] N. F. Mott and H. S. W. Massey, *The Theory of Atomic Collisions*, 3rd ed. (Clarendon, Oxford, 1965), p. 475.
[28] M. Inokuti, Rev. Mod. Phys. **43**, 297 (1971).
[29] D. R. Bates, A. Fundaminsky, and H. S. W. Massey, Philos. Trans. R. Soc. London, Ser. A **243**, 93 (1950); D. R. Bates, A. Fundaminsky, J. W. Leech, and H. S. W. Massey, *ibid.* **243**, 117 (1950).
[30] D. E. Shemansky, J. M. Ajello, D. T. Hall, and B. O. Franklin, Astrophys. J. **296**, 774 (1985).
[31] D. E. Shemansky, G. K. James, and J. A. Slevin, Astrophys. J. (to be published).
[32] D. R. Bates and A. Damgaard, Philos. Trans. R. Soc. London, A **242**, 101 (1949).
[33] W. J. Karzas and R. Latter, Astrophys. J. Suppl. **6**, 167 (1961).
[34] Kimball Physics, Inc., 311 Kimball Hill Road, Wilton, NH 03086-9742.
[35] J. M. Ajello, D. E. Shemansky, B. O. Franklin, J. Watkins, S. Srivastava, G. K. James, W. T. Simms, C. W. Hord, W. Pryor, W. McClintock, V. Argabright, and D. Hall, Appl. Opt. **27**, 890 (1988).
[36] G. K. James, J. M. Ajello, I. Kanik, B. O. Franklin, and D. E. Shemansky, J. Phys. B **25**, 1481 (1992).
[37] Lab Windows, National Instruments, 6504 Bridge Point Parkway, Austin, TX 78730-5039.
[38] J. A. Slevin and W. Stirling, Rev. Sci. Instrum. **52**, 1780 (1981).
[39] P. N. Clout and D. W. O. Heddle, J. Opt. Soc. Am. **59**, 715 (1969).
[40] F. G. Donaldson, M. A. Hender, and J. W. McConkey, J. Phys. B **5**, 1192 (1972).
[41] S. C. McFarlane, J. Phys. B **7**, 1756 (1974).
[42] I. C. Percival and M. J. Seaton, Philos. Trans. R. Soc. London Ser. A **251**, 113 (1958).
[43] J. L. Forand, S. Wang, J. M. Woolsey, and J. W. McConkey, Can. J. Phys. **66**, 349 (1988).
[44] J. M. Woolsey, J. L. Forand, and J. W. McConkey, J. Phys. B **19**, L493 (1986).
[45] D. E. Shemansky and G. R. Smith, J. Geophys. Res. **86**, 9179 (1981).
[46] B. Van Zyl and M. W. Gealy, Phys. Rev. A **35**, 3741 (1987).
[47] B. Van Zyl, B. K. Van Zyl, and W. B. Westerveld, Phys. Rev. A **37**, 4201 (1988).
[48] D. E. Shemansky, J. M. Ajello, and D. T. Hall, Astrophys. J. **296**, 765 (1985).
[49] D. W. O. Heddle, in *Advances in Atomic and Molecular Physics*, edited by D. R. Bates and B. Bederson (Academic Press, New York, 1979), Vol. 15, p. 381.
[50] M. E. Rudd, M. W. Gealy, G. W. Kirby III, and Y-Y. Hsu, Phys. Rev. Lett. **68**, 1504 (1992).
[51] E. M. Purcell, Astrophys. J. **116**, 457 (1952).
[52] P. O. Taylor, K. T. Dolder, W. E. Kauppila, and G. H. Dunn, Rev. Sci. Instrum. **45**, 538 (1974).
[53] K. H. Schartner (private communication).